*Tellus (2007), 59B, 179–190*
*Printed in Singapore. All rights reserved*



**TELLUS**

# Global monthly $CO_2$ flux inversion with a focus over North America

*By* FENG DENG[1]*, JING M. CHEN[1], MISA ISHIZAWA[1], CHIU-WAI YUEN[1], GANG MO[1], KAZ HIGUCHI[2], DOUGLAS CHAN[2] and SHAMIL MAKSYUTOV[3], [1]*Department of Geography, University of Toronto, 100 St. George Street, Toronto, Ontario, Canada M5S 3G3;* [2]*Meteorological Service of Canada, EC, 4905 Dufferin Street, Toronto, ON, Canada M3H 5T4;* [3]*National Institute of Environmental Studies, 16-2 Onogawa, Tsukuba, 305-8506, Japan*

(Manuscript received 15 January 2006; in final form 26 September 2006)

ABSTRACT

A nested inverse modelling system was developed for estimating carbon fluxes of 30 regions in North America and 20 regions for the rest of the globe. Monthly inverse modelling was conducted using $CO_2$ concentration measurements of 3 yr (2001–2003) at 88 sites. Inversion results show that in 2003 the global carbon sink is $-2.76 \pm 0.55$ Pg C. Oceans and lands are responsible for 88.5% and 11.5% of the sink, respectively. Northern lands are the largest sinks with North America contributing a sink of $-0.97 \pm 0.21$ Pg C in 2003, of which Canada's sink is $-0.34 \pm 0.14$ Pg C.

For Canada, the inverse results show a spatial pattern in agreement, for the most part, with a carbon source and sink distribution map previously derived through ecosystem modelling. However, discrepancies in the spatial pattern and in flux magnitude between these two estimates exist in certain regions. Numerical experiments with a full covariance matrix, with the consideration of the error structure of the a priori flux field based on meteorological variables among the 30 North America regions, resulted in a small but meaningful improvement in the inverted fluxes. Uncertainty reduction analysis suggests that new observation sites are still needed to further improve the inversion for these 30 regions in North America.

## 1. Introduction

Carbon dioxide, the most important greenhouse gas influenced by human activities and widely considered to be largely responsible for global warming, has been increasing steadily in the atmosphere (Keeling et al., 2005). Information on the spatial and temporal distributions of the carbon flux is critical to understanding and managing, if possible, the carbon cycle. Currently three approaches, including direct measurements (Wofsy et al., 1993; Takahashi et al., 1999), ecosystem modelling (Sellers et al. 1986 and 1996; Running and Coughlan, 1988 and Running and Gower, 1991; Potter and Klooster, 1999; Liu et al., 1999), and atmospheric inverse modelling (Kaminski et al., 1999; Rödenbeck et al., 2003; Gurney et al., 2003 and 2004; Baker et al., 2006) are used to estimate regional and global carbon fluxes. Inverse techniques compare simulated $CO_2$ concentrations in the atmosphere using an atmospheric transport model with observations at discrete sites over the globe. The spatial and temporal distributions of the difference between the simulated and observed values are used to infer the spatial and temporal patterns of the carbon flux.

However, the number of currently available observation stations is still sparse relative to the size of the global surface, and this essentially limits the number of regions that can be reliably inverted globally without using additional information as constraints to the inversion. The inverse technique that has been most commonly employed to estimate the carbon flux, the Bayesian synthesis inversion (Enting, 2002), requires a prior estimate of the carbon flux in each region to be inverted in order to balance the impacts of the errors in $CO_2$ observation and in the transport model on the final inverted carbon flux.

Spatial and temporal resolutions are other important aspects in inverse modelling, as we generally desire accurate spatial and temporal carbon cycle information for scientific and policy purposes. During the last decade, most inverse studies were done for large regions (<30 regions globally) (Enting et al., 1995; Fan et al., 1998; Rayner et al., 1999; Bousquet et al. 2000; Gurney et al., 2003) with several exceptions such as Kaminski et al. (1999), and Rödenbeck et al. (2003), who conducted inversions on a grid system with a resolution of approximately $8^\circ \times 10^\circ$. Due to their computation efficiency, the former approaches can be implemented easily in producing transport matrices and in

*Corresponding author.
e-mail: dengf@geog.utoronto.ca
DOI: 10.1111/j.1600-0889.2006.00235.x

solving the flux for each region. However, the aggregation errors for large regions may be of the same order of magnitude as the fluxes themselves (Kaminski et al., 2001), and we must be cautious in using the inverted fluxes to answer practical questions. On the other hand, the heavy computation load of high-resolution inversion may often be prohibitive, even though the aggregation errors are small for small regions. Through high-resolution inversion using 35 observation sites after a strict screening procedure, Rödenbeck et al. (2003) concluded that $CO_2$ fluxes can only be reliably inverted at continental to subcontinental scales.

Up to now, existing inversion results are too coarse in spatial resolution to be compared with other sources of information. For example, recent studies using different approaches show inconclusive and somewhat contradicting results on the net exchange of carbon between Canada's forests and the atmosphere. A study based on forest inventory by Kurz and Apps (1999) indicates Canada's forests to be a weak source (0.08 Pg C $yr^{-1}$) during the 1980s and 1990's. On the other hand, results through ecosystem modelling by Chen et al. (2000, 2003) found Canada's forests to be a weak sink ($-0.05$ Pg C $yr^{-1}$) in the same period. Global annual carbon flux inversions using atmospheric tracer transport models also yielded moderate flux information over North America boreal forests, and a source of $0.26 \pm 0.39$ Pg C $yr^{-1}$ during 1992–1996 was estimated in a TransCom 3 experiment (Gurney et al., 2003), while Fan et al. (1998) found it to be a sink of $-0.2 \pm 0.4$ Pg C $yr^{-1}$ during 1988–1992. Repeating the TransCom 3 (Level 1) experimental protocol, but with inclusion of the Fraserdale $CO_2$ data from 1992–1996, Yuen et al. (2005) obtained a flux estimate of $-0.003 \pm 0.28$ Pg C $yr^{-1}$ for the North American boreal region (Alaska and most of Canada). However, the coarse spatial resolution of these results does not allow determining the flux for specific regions within the boreal forest in Canada. An inversion with a higher resolution over North America is therefore of great interest in advancing our understanding of regional carbon cycles. However, if we only carry out inversion over North America, fluxes of $CO_2$ across the boundaries of the region would become a major issue. A global inversion in a fine grid would be ultimately the best way to improve inversion results, but it is currently computationally prohibitive. We therefore developed a nested inversion framework of 50 global regions with 30 small regions over North America based on a land cover map at 1 km resolution derived from AVHRR Data (DeFries and Townshend, 1994) as a compromise. We aim at improving our estimates for North America in two ways: (i) defining regions based on land cover type to reduce the error caused by the heterogeneity inside a region, and (ii) inverting smaller regions than TransCom 3 to reduce the aggregation errors. In order to provide continuity with TransCom 3 results, we chose to use the same 22 regions of the globe as used in TransCom 3, except that two North America regions were divided into 30 small regions (See Fig. 1).

Here, we present seasonal inversion results of 2003 based on the $CO_2$ measurements made from 2001 to 2003. Section 2 provides a description of the method employed, including the transport model used in this study, the inversion set-up, and observation data. In Section 3, we present the results of this study, including the annual flux and its uncertainty, and seasonal fluxes and their uncertainties for each region. Meanwhile, comparisons are also made between our results and the TransCom 3 annual (Gurney et al., 2003), seasonal (Gurney et al., 2004), and interannual (Baker et al., 2006) inversion results. We also identify possible directions for future improvements for nested global inversion.

## 2. Inversion methods

### 2.1. Time-dependent Bayesian synthesis method

To estimate carbon fluxes ($\mathbf{f}$), we represent the relationship between $CO_2$ measurements and site observations by a linear model:

$$\mathbf{c} = \mathbf{G}\mathbf{f} + \mathbf{A}c_0 + \varepsilon, \tag{1}$$

where $\mathbf{c}_{m\times 1}$ is a given vector of $CO_2$ concentrations; $\varepsilon_{m\times 1}$ is a random error vector with a zero mean and a covariance matrix $\mathrm{cov}(\varepsilon) = \mathbf{R}_{m\times m}$; $\mathbf{G}_{m\times(n-1)}$ is a given matrix representing a transport operator; $\mathbf{A}_{m\times 1}$ is a vector filled with 1 relating to the assumed initial well-mixed atmospheric $CO_2$ concentrations ($c_0$) of at least two years before the first observation month; and $\mathbf{f}_{(n-1)\times 1}$ is an unknown vector of carbon fluxes of all studied regions. Combining matrix $\mathbf{G}$ and $\mathbf{A}$ as $\mathbf{M}_{m\times n} = (\mathbf{G}, \mathbf{A})$, and vector $\mathbf{f}$ and $c_0$ as $\mathbf{s}_{n\times 1} = (\mathbf{f}^{\mathbf{T}}, c_0)^{\mathbf{T}}$, eq. (1) can be expressed as

$$\mathbf{c} = \mathbf{M}\mathbf{s} + \varepsilon. \tag{2}$$

If matrix $\mathbf{M}$ is ill conditioned, i.e. $m < n$, we cannot solve the equations with the traditional least square approach. Even if we have more or equal measurement equations than the unknown variables ($m \geq n$) in the equations, as the case in this experiment, we still may not obtain a reliable solution of the unknown fluxes constrained only by the $CO_2$ measurement because of the uncertainty of $CO_2$ concentration measurement, transport model errors, the uneven distribution of measurement sites, and different region sizes which may make the problem poorly constrained in some regions where we have relatively few measurement sites and overconstrained over other regions where we have many measurement sites. In this case, the following objective function

$$J = \frac{\mathbf{1}}{\mathbf{2}}(\mathbf{M}\mathbf{s} - \mathbf{c})^{\mathbf{T}}\mathbf{R}^{-\mathbf{1}}(\mathbf{M}\mathbf{s} - \mathbf{c}) + \frac{\mathbf{1}}{\mathbf{2}}(\mathbf{s} - \mathbf{s_p})^{\mathbf{T}}\mathbf{Q}^{-\mathbf{1}}(\mathbf{s} - \mathbf{s_p}) \tag{3}$$

is employed in place of the traditional least square objective function, where $\mathbf{s_p}_{n\times 1}$ is the a priori estimate of $\mathbf{s}$; the covariance matrix $\mathbf{Q}_{n\times n}$ represents the uncertainty in the a priori estimate; and $\mathbf{R}_{m\times m}$ is the model-data mismatch error covariance. By minimizing this objective function, eq. (3), we obtain the posterior best estimate of $\mathbf{s}$ as:

$$\hat{\mathbf{s}} = (\mathbf{M}^{\mathbf{T}}\mathbf{R}^{-\mathbf{1}}\mathbf{M} + \mathbf{Q}^{-\mathbf{1}})^{-\mathbf{1}}(\mathbf{M}^{\mathbf{T}}\mathbf{R}^{-\mathbf{1}}\mathbf{c} + \mathbf{Q}^{-\mathbf{1}}\mathbf{s_p}). \tag{4}$$

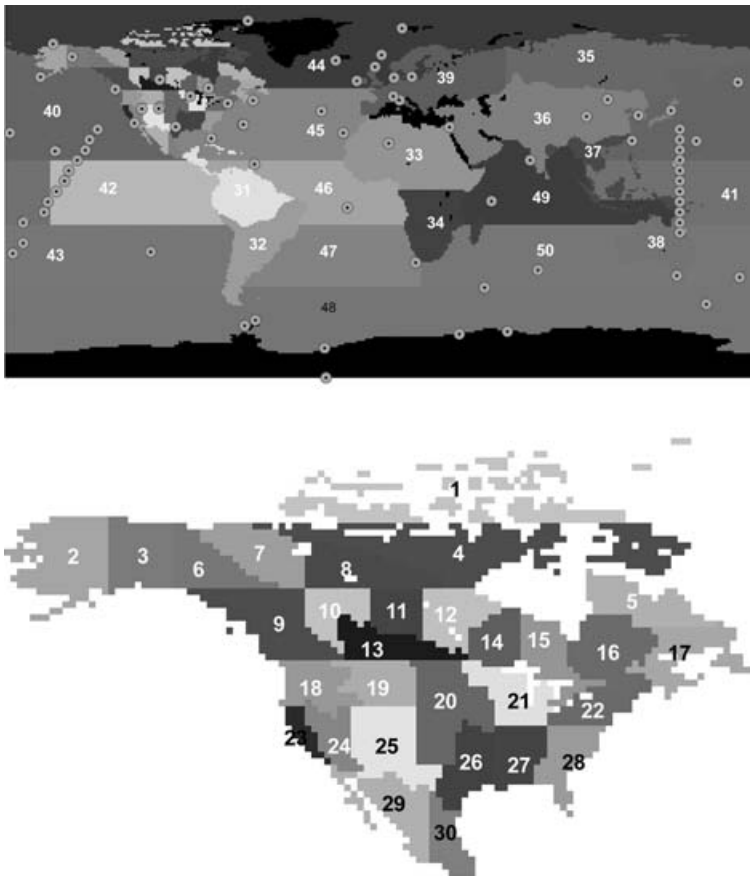


*Fig 1.* A nested inversion scheme: 30 regions in North America and 20 regions for the rest of the globe. Locations of 88 $CO_2$ observational sites are also indicated.

Meanwhile the posterior uncertainty matrix of the posterior flux can be written as:

$$\hat{\mathbf{Q}} = (\mathbf{Q^{-1}} + \mathbf{M^T R^{-1} M})^{-1}. \quad (5)$$

The measure we employed to check the fit to the observations requires the modelled $CO_2$ concentration, on average, within $\pm\sqrt{R_{ii}}$ (see eq. (7)) from the observations (Rödenbeck et al., 2003).

### 2.2. *Transport modelling*

The NIES (National Institute of Environmental Studies of Japan) global transport model (Maksyutov and Inoue, 2000), one of the TransCom 3 participating models, was used to simulate the monthly tracer pulse functions. The model has 15 levels in the sigma coordinate and a 2.5° × 2.5° horizontal resolution. The transport model was forced by the six-hourly NCEP/NCAR reanalysis data (Kalnay et al. 1996). By coupling with Biome-BGC (Thornton et al. 2002), a process-based ecosystem model which is driven by daily meteorological data derived from NCEP/NCAR reanalysis data, monthly transport operator matrices of five years (1999–2003) for the 50 regions were produced. That means for each month and region, a flux pattern (normalized to 1 Pg C $yr^{-1}$) is prescribed in the NIES model for forward transport computation to determine the contribution of each region to the $CO_2$ concentration at each observation site since January of 1999 in order to form the G matrix (3168 × 3000). The three background fluxes, (i) the 1995 fossil fuel emission field (Brenkert, 1998), (ii) the neutral seasonal biosphere exchange based on the Biome-BGC model (Thornton et al., 2002), and (iii) the air–sea gas exchange (Takahashi et al., 1999), were considered in the forward transport modelling to calculate the pre-subtracted portions of the $CO_2$ concentration in the same way as they were treated in the TransCom 3 seasonal inversion (Gurney et al., 2004). The actual pre-subtracted portions of the $CO_2$ concentration caused by fossil fuel emission from 2001 to 2003 are adjusted linearly according to the global fossil fuel emission from 1995 to 2003 (Marland, Boden, and Andres, 2006). If we substitute **c** in eq. (1) with the differences of the monthly means of observed $CO_2$ concentration and these pre-subtracted portions, then **f** in eq. (1) will be the differences between the carbon fluxes and pre-subtracted fluxes.

The selection of a proper atmospheric transport model would be critical to the accuracy of inversion. However, Baker et al. (2006) found that the uncertainty introduced into the inverted fluxes due to transport error (with all of the TransCom 3 participating models) is generally less than the random estimation error. We have therefore used only one model in this study with

full understanding that the uncertainty in the results would be larger than the case with an ensemble of models.

### 2.3. Prior fluxes, and their uncertainties

The same seasonally varying a priori regional flux magnitudes used in TransCom 3 seasonal inversion (Gurney et al., 2004) have been used here with those 20 large regions. For the small regions in North America, we distributed the a priori flux for each region based on a multi-year mean of NEP (Potter et al., 2003) while keeping the sum of the a priori for all 30 regions equal to that of the two large TransCom 3 regions in North America.

A reasonable estimate of the prior flux uncertainty is important for deriving inverted results that are close to reality. Based on previous studies (Gurney et al., 2004; Rödenbeck et al., 2003; Michalak et al., 2004; Baker et al., 2006), we adopted two approaches to determine the covariance matrix for the a priori surface flux.

(1) As a basic approach, we used a diagonal matrix with all its elements filled with the TransCom 3 interannual variability version prior flux uncertainty ($\sigma$) (Baker et al., 2006) for the large regions. For those small regions we re-constructed the uncertainties for each region according to the same principle that have been used for those large regions in TransCom 3 seasonal inversion (Gurney et al., 2004).

(2) As an experimental approach, we defined the covariance items as:

$$Q_{ij} = w \cdot C_{ij} \cdot \sigma_{idiag} \cdot \sigma_{jdiag} \Bigg/ \left(1 + \frac{a \cdot |\Delta P_{ij}|}{\overline{P}} + \frac{b \cdot |\Delta T_{ij}|}{(30 + \overline{T})}\right), \quad (6)$$

where $C_{ij}$ is the correlation coefficient of NEP time series between regions $i$ and $j$ based on Biome-BGC; $\sigma_{idiag}$ is the diagonal variance of region $i$ used in the first approach; $\overline{P}$ and $\overline{T}$ are the mean precipitation and temperature of regions $i$ and $j$; $\Delta P_{ij}$ is the difference in precipitation between regions $i$ and $j$; $\Delta T_{ij}$ is the difference in temperature between regions $i$ and $j$; $a$, and $b$ are two empirical parameters to define the weights of precipitation and temperature, respectively; and $w$ is a parameter to ensure that all the related uncertainty elements in the covariance matrix represent the same uncertainties in the diagonal matrix. In this study, we chose $w = 0.5$ when $i = j$ to keep 50% of the diagonal terms, and distributed 50% of them to the off-diagonal terms. Choosing $a = 1$, we can obtain $b = 1.75$ to make the weights of both temperature and precipitation to be same on an annual basis. Finally we can obtain $w = 0.140367, 0.140212, 0.138309, 0.140135, 0.133965, 0.128556, 0.126129, 0.130530, 0.132317, 0.139378, 0.141208$ and $0.141596$ for 12 months, respectively, when $i \neq j$ for those small regions of North America. For other regions outside of North America we used the same diagonal elements.

The guiding principle in constructing this matrix is that in the nested inversion we do not have enough atmospheric $CO_2$ stations over North America, and that the spatial pattern of the prior surface flux could be used as a source of information to constrain the inversion for small regions. This constraint may be accomplished by the covariance of the errors between various small regions. If two regions have similar climate conditions, namely temperature and precipitation, we expect that the errors in the flux estimates for these two regions are better correlated than those of dissimilar climate conditions. This approach has been only applied to those small regions of 1 to 30 in North America for sensitivity analysis and will be further discussed in Section 3.2.

### 2.4. $CO_2$ concentration data and model-data mismatch error covariance matrix

We selected monthly mean $CO_2$ data of 2001 to 2003 at 88 sites (see Fig. 1 and Table 1) from the GLOBALVIEW-2005 dataset (GLOBALVIEW-$CO_2$, 2005). For regions outside of North America, most of the selected sites have been used in published inversions (Gurney et al., 2003; Rödenbeck et al., 2003; Baker et al., 2006; Patra et al., 2005). For North America, however, we have to select as many sites as possible in order to conduct meaningful inversion for the small 30 regions. The extended record files with extrapolated data (Masarie and Tans, 1995) were used to calculate the monthly mean $CO_2$ concentrations. Table 1 provides the percentage of observed ('real') $CO_2$ concentration data to the data we used in the inversion at each site.

We defined the data-mismatch error covariance as a diagonal matrix, R, and determined the error standard deviation of month $i$ by

$$R_{ii} = (0.175 ppmv)^2 + (GVsd)^2, \quad (7)$$

where $GVsd$ is the standard deviation of the residual distribution computed monthly from the average monthly variability (var) files of GLOBALVIEW-$CO_2$ 2005, and 0.175 ppmv is the systematic errors for all the data at each site. Table 1 lists the annual-mean of the monthly error standard deviations $\sqrt{R_{ii}}$ for all 88 sites.

We used a three-year series of $CO_2$ observations to invert the flux in 2003 because we need enough time to spin-up the $CO_2$ distribution in the atmosphere. A spin-down period is also needed to better constrain the last few months of the inversion, but this is not considered in this study.

## 3. Results and discussion

### 3.1. Seasonal variation

Prior and inverted seasonal fluxes and prior and posterior uncertainties for all 50 individual regions are shown in Fig. 2.

*Table 1.* $CO_2$ dataset quality and the annual mean uncertainty of the 88 selected stations

| GlobalView-2005 Site ID | Percentage of observed data (%) 2001 | 2002 | 2003 | 3-year mean | Annual mean uncertainty (ppmv) | GlobalView-2005 Site ID | Percentage of observed data (%) 2001 | 2002 | 2003 | 3-year mean | Annual mean uncertainty (ppmv) |
|---|---|---|---|---|---|---|---|---|---|---|---|
| alt_06C0 | 100 | 100 | 100 | 100 | 0.79 | poc000_01D1 | 0 | 56.25 | 100 | 52.08 | 0.5 |
| ams_11C0 | 100 | 100 | 100 | 100 | 0.31 | pocn05_01D1 | 0 | 56.25 | 100 | 52.08 | 0.5 |
| asc_01D0 | 66.67 | 100 | 100 | 88.89 | 0.61 | pocn10_01D1 | 0 | 47.92 | 100 | 49.31 | 0.55 |
| ask_01D0 | 77.08 | 100 | 100 | 92.36 | 0.5 | pocn15_01D1 | 0 | 58.33 | 100 | 52.78 | 0.61 |
| azr_01D0 | 70.83 | 83.33 | 81.25 | 78.47 | 1.2 | pocn20_01D1 | 0 | 58.33 | 100 | 52.78 | 0.84 |
| bal_01D1 | 62.5 | 70.83 | 100 | 77.78 | 4.36 | pocn25_01D1 | 0 | 47.92 | 100 | 49.31 | 1.01 |
| bhd_15C0 | 95.83 | 0 | 0 | 31.94 | 0.35 | pocn30_01D1 | 0 | 50 | 100 | 50 | 1.1 |
| bme_01D0 | 100 | 100 | 100 | 100 | 1.42 | pocs05_01D1 | 0 | 56.25 | 100 | 52.08 | 0.53 |
| bmw_01D0 | 100 | 100 | 100 | 100 | 1.42 | pocs10_01D1 | 0 | 56.25 | 100 | 52.08 | 0.53 |
| brw_01C0 | 100 | 100 | 100 | 100 | 1.09 | pocs15_01D1 | 0 | 54.17 | 100 | 51.39 | 0.56 |
| car040_01D2 | 93.75 | 100 | 72.92 | 88.89 | 0.93 | pocs25_01D1 | 0 | 33.33 | 100 | 44.44 | 0.46 |
| car060_01D2 | 93.75 | 100 | 68.75 | 87.5 | 0.61 | pocs30_01D1 | 0 | 31.25 | 100 | 43.75 | 0.35 |
| cba_01D0 | 100 | 100 | 100 | 100 | 1.19 | prs_21C0 | 100 | 100 | 100 | 100 | 0.72 |
| cfa_02D0 | 60.42 | 100 | 100 | 86.81 | 0.75 | psa_01D0 | 100 | 100 | 100 | 100 | 0.24 |
| cgo_01D0 | 100 | 100 | 100 | 100 | 0.25 | rpb_01D0 | 100 | 100 | 100 | 100 | 0.52 |
| cmn_17C0 | 100 | 100 | 100 | 100 | 1.79 | ryo_19C0 | 100 | 100 | 100 | 100 | 1.61 |
| cpt_36C0 | 100 | 100 | 100 | 100 | 0.34 | sbl_06C0 | 0 | 0 | 56.25 | 18.75 | 2.34 |
| cri_02D0 | 100 | 77.08 | 0 | 59.03 | 1.71 | sey_01D0 | 100 | 100 | 100 | 100 | 0.74 |
| crz_01D0 | 79.17 | 47.92 | 45.83 | 57.64 | 0.29 | shm_01D0 | 100 | 100 | 100 | 100 | 0.93 |
| eic_01D0 | 100 | 100 | 41.67 | 80.56 | 0.59 | sis_02D0 | 100 | 100 | 93.75 | 97.92 | 0.85 |
| esp_06D0 | 81.25 | 64.58 | 100 | 81.94 | 2.15 | smo_01C0 | 100 | 100 | 100 | 100 | 0.48 |
| frd040_06C3 | 100 | 100 | 100 | 100 | 3.86* | spo_01C0 | 100 | 100 | 100 | 100 | 0.19 |
| gmi_01D0 | 100 | 100 | 100 | 100 | 0.77 | stm_01D0 | 100 | 100 | 100 | 100 | 1.05 |
| hba_01D0 | 100 | 100 | 100 | 100 | 0.21 | syo_09C0 | 100 | 95.83 | 0 | 65.28 | 0.19 |
| hfm005_01D2 | 93.75 | 87.5 | 66.67 | 82.64 | 3.50* | tap_01D0 | 100 | 100 | 100 | 100 | 2.93 |
| ice_01D0 | 100 | 79.17 | 100 | 93.06 | 1.03 | uta_01D0 | 100 | 100 | 100 | 100 | 1.73 |
| izo_27C0 | 100 | 100 | 0 | 66.67 | 0.76 | uum_01D0 | 100 | 83.33 | 100 | 94.44 | 1.61 |
| jbn_29C0 | 100 | 100 | 100 | 100 | 0.38 | wes_23C0 | 79.17 | 100 | 8.33 | 62.5 | 2.43 |
| key_01D0 | 100 | 100 | 100 | 100 | 0.83 | wis_01D0 | 100 | 100 | 100 | 100 | 1.77 |
| kum_01D0 | 100 | 100 | 100 | 100 | 0.77 | wkt030_01C3 | 87.5 | 100 | 58.33 | 81.94 | 3.74 |
| lef011_01C3 | 100 | 93.75 | 0 | 64.58 | 3.94 | wlg_33C0 | 89.58 | 43.75 | 100 | 77.78 | 1.16 |
| lef076_01C3 | 100 | 93.75 | 0 | 64.58 | 3.84 | wpo000_10D2 | 100 | 100 | 89.58 | 96.53 | 0.36 |
| lef122_01C3 | 100 | 93.75 | 0 | 64.58 | 3.81 | wpon05_10D2 | 100 | 100 | 89.58 | 96.53 | 0.35 |
| lef244_01C3 | 100 | 93.75 | 0 | 64.58 | 3.74 | wpon10_10D2 | 100 | 100 | 89.58 | 96.53 | 0.32 |
| ljo_04D0 | 100 | 4.17 | 0 | 34.72 | 2.73* | wpon15_10D2 | 100 | 100 | 89.58 | 96.53 | 0.33 |
| maa_02D0 | 100 | 41.67 | 100 | 80.56 | 0.24 | wpon20_10D2 | 100 | 100 | 89.58 | 96.53 | 0.37 |
| mhd_01D0 | 100 | 100 | 100 | 100 | 1.3 | wpon25_10D2 | 100 | 100 | 89.58 | 96.53 | 0.47 |
| mid_01D0 | 100 | 100 | 100 | 100 | 0.91 | wpon30_10D2 | 100 | 100 | 89.58 | 96.53 | 0.55 |
| mlo_01C0 | 100 | 100 | 100 | 100 | 0.47 | wpos05_10D2 | 100 | 100 | 89.58 | 96.53 | 0.4 |
| mnm_19C0 | 100 | 100 | 100 | 100 | 0.86 | wpos10_10D2 | 100 | 100 | 89.58 | 96.53 | 0.43 |
| mqa_02D0 | 100 | 100 | 100 | 100 | 0.29 | wpos15_10D2 | 100 | 100 | 89.58 | 96.53 | 0.47 |
| nwr_01D0 | 100 | 100 | 100 | 100 | 1.08 | wpos20_10D2 | 100 | 100 | 89.58 | 96.53 | 0.43 |
| obs023_06C3 | 0 | 0 | 97.92 | 32.64 | 3.49* | yon_19C0 | 100 | 100 | 100 | 100 | 1.41 |
| pfa025_01D2 | 64.58 | 62.5 | 75 | 67.36 | 0.73 | zep_01D0 | 100 | 100 | 100 | 100 | 1.06 |

*Adjustment has been made on the uncertainty.

More than half of the posterior curves are changed significantly from the a priori curve, suggesting the effectiveness of atmospheric constraint. Among the large regions outside of North America, several changes are noteworthy. The major heat wave and drought (NCDC, 2004) in Europe (Region 39), for example, may be the reason that the posterior flux curve shifts upward during summer and fall seasons. The continued drought in South Africa (Region 34) may be the cause for shifting the a priori

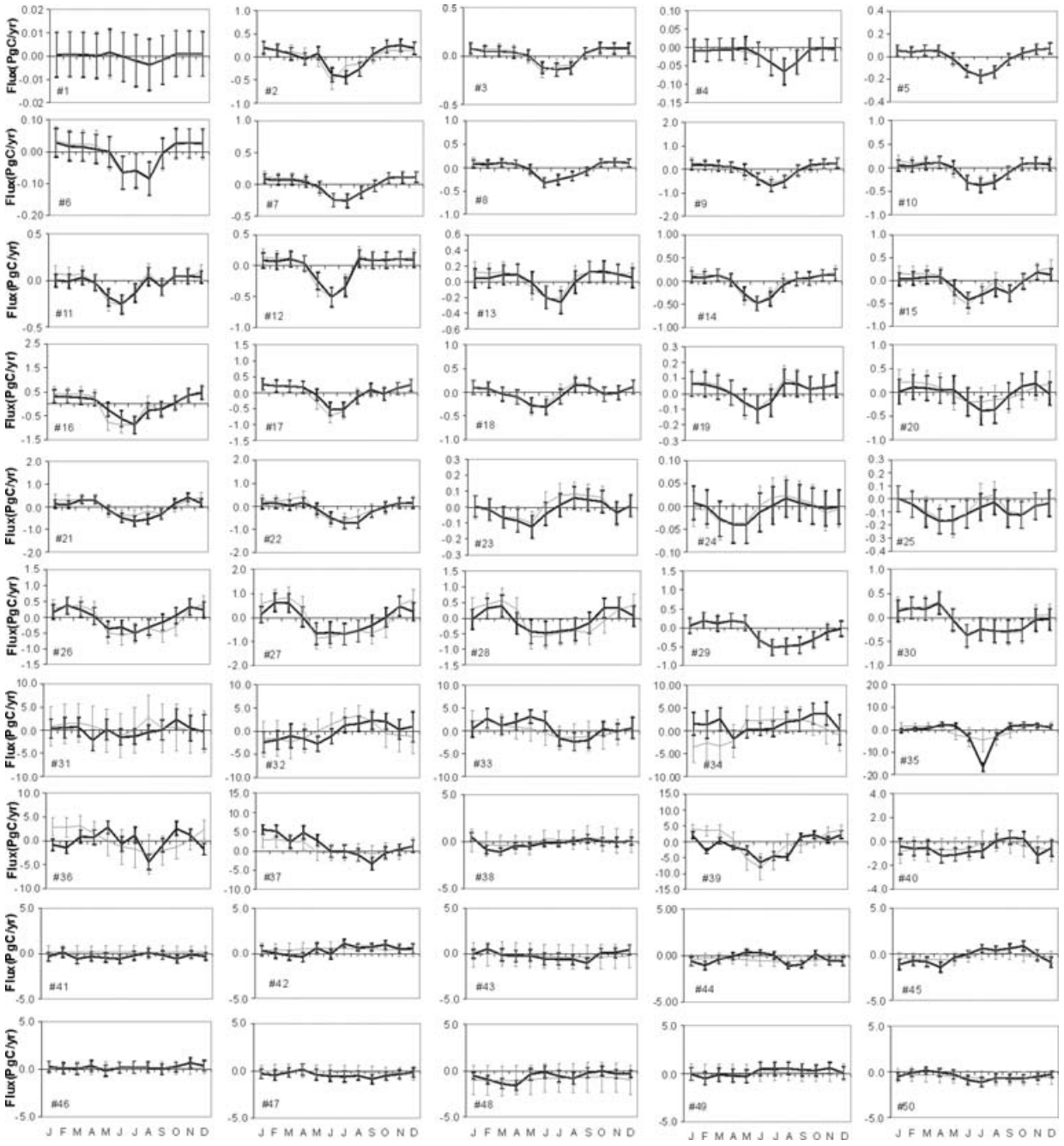


*Fig 2.* Seasonal patterns of the a priori flux (grey) and the inverted flux (dark) for the 50 regions and their uncertainties of 2003.

carbon uptake in the first three months to posterior carbon release. In Region 36, the May/June heat wave (NCDC, 2004) might be one of the reasons that the carbon uptake is delayed until July and August. Although we cannot explain all the differences in all regions, these examples suggest that our inversion is meaningful.

The magnitude of the decrease from the prior uncertainty to the posterior uncertainty indicates the degree to which the final inverted flux is constrained by $CO_2$ measurements. From Fig. 2, we can see the uncertainty reduction for each month and region. In order to investigate the uncertainty reduction in different regions, we defined the uncertainty reduction percentage ($U_R$) as follow:

$$U_R = \frac{q - q'}{q} \times 100\%, \tag{8}$$

where $q$ is the a priori flux uncertainty for a region in 2003, which equals the square root of the sum of the 12 related diagonal items

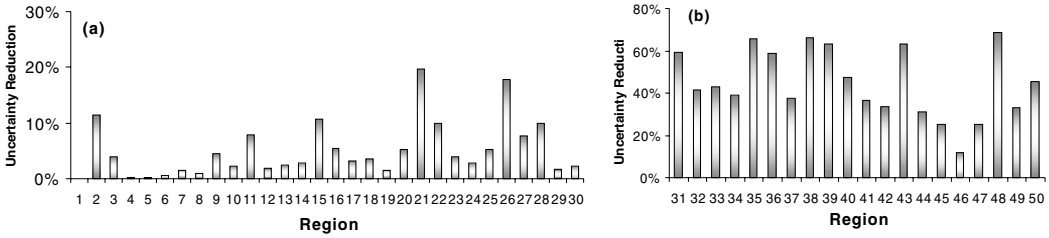


*Fig 3.* Annual flux uncertainty change for all inverted regions. (a) North America. (b) Regions outside of North America.

of $\mathbf{Q}$ in eq. (3); and $q'$ is the posterior flux uncertainty for a region, which equals the square root of the sum of a sub-matrix related to the 12 months of $\hat{\mathbf{Q}}$ defined in eq. (5). Figs. 3(a) and 3(b) present the uncertainty reduction percentages for all 50 regions.

The Tropical Atlantic Ocean (Region 46) exhibits the smallest reduction in the uncertainty mainly due to the few reliable observation sites exist in or around the region in comparison with other ocean regions (table 1). Of course the a priori uncertainty is also a factor affecting the uncertainty reduction. It is often those regions with large a priori uncertainties and constrained by a sufficient number of good observation sites show large reductions in uncertainty. The South Pacific Ocean (Region 43), and the Southern Ocean (Region 48), for example, have the greatest reductions of the uncertainty. For the land regions, we have to separate them into two groups for comparison because of the influence of a priori uncertainty on the uncertainty reduction. For large land regions, the largest reduction of the uncertainty appears in extra-tropical part of Eurasia continent. This can be attributed to the relatively large number of reliable observation sites in these regions, in contrast with fewer sites in the tropical and southern land regions (excluding Region 38). For the 30 small regions in North America, a general impression is that reductions in uncertainty are smaller than the large regions. One of the reasons is that we assigned relatively small a priori uncertainty for the small regions. In most northern regions containing no land observing sites, the uncertainty reductions are very small. There are also little uncertainty reductions in several southern regions, such as Regions 19, and 29. However, if we consider North America as one region, the uncertainty reduction can be as large as 33.4%. This total uncertainty reduction for this large region is much larger than the mean value of the small 30 regions because of covariance among small regions, leading to a posterior uncertainty of 0.21 Pg C $yr^{-1}$ for North America.

In our inversion estimate, there is a time lag in the seasonal cycle between our inverted flux and the a priori flux for northern land regions. As Biome-BGC is driven by meteorological variables, we expect that carbon fluxes resulting from photosynthesis activities would lag behind the flux estimation of Biome-BGC based on air temperature because the seasonal increase or decrease in soil temperature would lag behind the air temperature. Comparing observed $CO_2$ concentration and those simulated from forward transport modelling using Biome-BGC flux, Zhang et al. (2005) also noticed a similar phase lag.

### 3.2. Annual distribution

Monthly carbon fluxes presented in Fig. 2 are summed to yield a spatial distribution of the annual net flux, as shown in Fig. 4. From this map, the performance of our inversion can be evaluated. The northern land is a large carbon sink of $-3.14 \pm 0.34$ Pg C $yr^{-1}$, and the tropical land and the southern land are carbon sources of $1.82 \pm 0.67$ and $1.01 \pm 0.68$ Pg C $yr^{-1}$, respectively.

As our nested inversion is considered as an extension of TransCom 3, we first compared our annual results with TransCom 3 results. Fig. 5 shows the annual results from (a) this inversion for 2003, (b) the NIES model results in TransCom 3 seasonal inversion from 1992 to 1996 (Gurney et al., 2004), (c) the NIES model alone used in TransCom 3 annual inversion from 1992 to 1996 (Gurney et al., 2003), and the NIES model flux results for 2003 from the TransCom 3 interannual variability study (Baker et al., 2006). The region NA represents the combination of Regions 1 to 30 in this inversion, which is a combination of the Boreal North America and Temperate North America in TransCom 3.

Although the inverted fluxes represent different time periods, North America (NA), Europe (39), and Asia Boreal (35) were the most important carbon sinks over land regions, while Southern Africa (34) and Tropical Asia (37) were carbon sources. For the Europe region (39), the inverted sink from this inversion ($1.17 \pm 0.27$ Pg C $yr^{-1}$) is smallest among the four inverted results and is only 69% of the estimate from TransCom 3 seasonal inversion ($-1.69 \pm 0.16$ Pg C $yr^{-1}$), while the result from the TransCom 3 interannual inversion is almost the same as the TransCom 3 annual inversion ($-1.22 \pm 0.35$ Pg C $yr^{-1}$). We can also find that the curve of the monthly flux (Fig. 2) differs notably from the TransCom 3 seasonal estimation curve (Gurney et al., 2004), which may reflect the anomaly of 2003 in this region (Ciais et al., 2005). For the Asia Boreal region (35), our inversion result ($-0.95 \pm 0.27$ Pg C $yr^{-1}$) differs most from that of the TransCom 3 annual inversion ($-1.34 \pm 0.37$ Pg C $yr^{-1}$) and least from the TransCom 3 interannual result ($-0.97$ Pg C $yr^{-1}$). The uptake ($-0.97 \pm 0.21$ Pg C $yr^{-1}$) for North America from our inversion is the largest, while TransCom 3 interannual inversion produced a sink of $-0.61$ Pg C $yr^{-1}$, which is the second largest. We found greater disagreement than the above cases in other land regions, especially in the Africa continent. The Northern Africa region (33) only releases less than 1/3 of TransCom 3 interannual

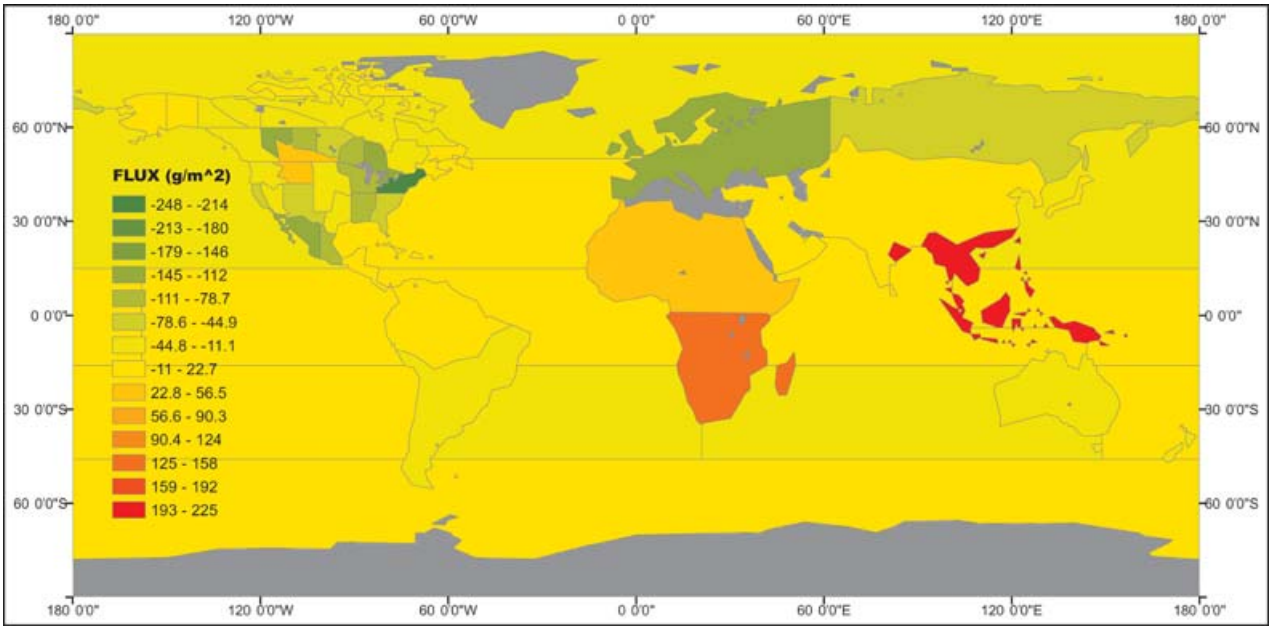


*Fig 4.* The inverted annual carbon flux distributions in 2003, including pre-subtracted ocean flux, excluding fossil fuel emission.

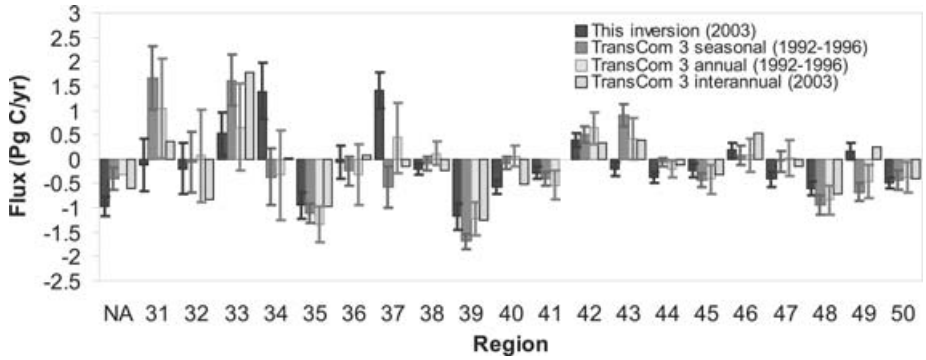


*Fig 5.* Comparison of nested monthly step inversion results from this study with NIES model results from TransCom 3 seasonal inversion (1992–1996) (Gurney et al., 2004), NIES model results from TransCom 3 annual inversion (1992–1996) (Gurney et al., 2003), and NIES model results from the TransCom 3 interannual variability study (2003) (Baker et al., 2006). Region NA represents the combination of Regions 1 to 30 in this inversion, which is the same as the combination of Boreal NA and Temperate NA of TransCom 3.

inversion results, while the Southern Africa region (34) becomes a large source in our inversion, opposite to TransCom 3 annual and seasonal results. However, if we put the Northern Africa region (33) and the Southern Africa region (34) together, the carbon release from the whole continent would be in good agreement with the results from TransCom 3 seasonal and interannual inversions. The possible reason could be the different observation sites selected in or around these regions. The continued drought and abnormal wildfire events in the Southern Africa region (34) and the above normal rainfall in the Northern Africa region (33) may also have some contributions to the differences among the inversion results.

The largest change appears in Tropical America (31) where the TransCom 3 seasonal inversion shows a carbon release of $1.67 \pm 0.66$ (Pg C $yr^{-1}$), the largest of all 50 regions, while this study gives a small sink of $-0.11 \pm 0.55$ (Pg C $yr^{-1}$), which differs the least from the result (0.37 Pg C $yr^{-1}$) of Baker et al. (2006).

For ocean regions our inversion mostly shows a very similar pattern with the TransCom 3 interannual results, and in close agreement with the result of Takahashi et al. (1999), one of our pre-subtracted components. However, in the Tropical West Pacific region (41), the South Atlantic region (47), and the Southern Ocean region (48), we found obvious differences. In the Southern Ocean region (48), our result ($-0.61 \pm 0.14$ Pg C $yr^{-1}$) only shows less than 70% of the uptake of Takahashi et al. (1999), and it is close to the new result ($-0.40 \pm 0.35$ Pg C $yr^{-1}$) of Gruber et al. (2005), while the TransCom 3 (NIES) results are in close agreement with the sink value of Takahashi et al. (1999). The southern Pacific region (43) shows the largest difference of

1.11 Pg C $yr^{-1}$ from the seasonal and more than 0.5 Pg C $yr^{-1}$ from the annual and the interannual result of TransCom 3, and this may be due to the inclusion of the Easter Island site in our inversion (Law et al., 2003).

For inverted fluxes in the 30 small regions in North America (Figure 4), no other similar inversion results are available for comparison. However, it is encouraging to see that the distribution pattern of sinks and sources in Canada seems to resemble 'bottom-up' results of 1990–1998 independently estimated based on remote sensing and other spatial datasets (Chen et al., 2003; Chen et al., 2005; and Ju et al., 2006). The 'bottom-up' results show that Region 10, the forested region of Albert, Canada, and Regions 14, 15 and 16, the mid-age productive forests in southern Ontario and Quebec were obvious carbon sinks, while our result of 2003 shows that Regions 10 and 15 are the strongest sinks of $-117.29 \pm 88.09$ and $-117.94 \pm 77.86$ g C $m^{-2}$ $yr^{-1}$, respectively. Region 9, in west of Canada, is a small carbon sink due to the old age forest in the 'bottom-up' result, while our inversion result shows that it is a weak sink of $-38.01 \pm 66.47$ g C $m^{-2}$ $yr^{-1}$. Region 12, the forested regions of Manitoba, was found to be carbon sources due to frequent fire disturbance in recent decades, while our result of 2003 shows that Region 12 is a weak sink of $47.90 \pm 70.73$ g C $m^{-2}$ $yr^{-1}$. From the respect of relative strength of whole Canada, the spatial patterns from this study are broadly consistent with the `bottom-up' results.

However, we found considerable relative differences in Regions 11, 16 and 17. Our results shows that Region 11 is a strong sink of $-106.15 \pm 64.45$ g C $m^{-2}$ $yr^{-1}$, Region 16 is a weak sink of $-36.54 \pm 101.03$ g C $m^{-2}$ $yr^{-1}$, and region 17 is a weak source of $4.64 \pm 77.13$ g C $m^{-2}$ $yr^{-1}$. To investigate the reason for these discrepancies, we experimented with different a priori flux uncertainty matrices including the full covariance matrix as defined in equation (6). The full covariance matrix made small but non-negligible differences in the inverted flux distribution (Fig. 6), and in Region 17, it produces a sink of $-20.58 \pm 54.68$ g C $m^{-2}$ $yr^{-1}$; in Region 16, the sink is strengthened to $59.09 \pm 70.94$ g C $m^{-2}$ $yr^{-1}$; in Region 11, the sink strength also decreases to $93.40 \pm 46.51$ g C $m^{-2}$ $yr^{-1}$. The sensitivity experiment demonstrates that the use of the a priori flux uncertainty covariance matrix can reduce the posterior flux uncertainty, especially for those poorly constrained regions (Fig. 6). The mean posterior uncertainty of all 30 North America regions is further reduced by 7.6% in contrast with that of the well-constrained regions (2, 11, 15, 21, 22 and 26) when comparing with the case that only the diagonal a priori error matrix is used. This suggests that a full covariance matrix would allow regions that are not well constrained by atmospheric measurements to be reliably inverted as the covariance between biologically similar regions can provide the additional source of spatial information. It is therefore critical to understand the behaviour of an ecosystem model in terms of their error structure.

For northern regions in Canada, where there are not enough observation sites, the number of the observation stations is therefore the main limiting factor in the inversion, in particular for regions where the surface flux has little impacts on concentrations at existing stations. For example, the inverted fluxes of Regions 4, 5 and 6 are mostly controlled by the a priori fluxes. This reinforces the existing argument that tall tower $CO_2$ measurements at continental sites are critical for quantifying regional carbon budgets (Yuen et al., 2005). From the effect of adding one observation site - Old Black Spruce, Saskatchewan, Canada, in Region 11 on the inversion results, we may conclude that adding three or more observation sites in North America would greatly enhance our nested inversion accuracy.

### *3.3. Global and North America carbon budget*

Compared with results of previous seasonal and annual inversions (1992–1996), and interannual inversion (in2003) of TransCom 3, this inversion derives a similar carbon uptake by the Earth's surface. The net total flux from the atmosphere, excluding fossil fuel emissions (7.303 Pg C) but including emissions associated with land use changes, is a sink of $-2.76 \pm 0.55$ Pg C in 2003 from this inversion, a sink of $-2.81 \pm 0.01$ Pg C $yr^{-1}$ (1992 –1996) from the NIES model in TransCom 3 seasonal inversion (Gurney *et al*. 2004), and $-2.47$ Pg C in 2003 from the NIES model in the interannual inversion of TransCom 3 excluding fossil fuel emission of 7.0 Pg C (Baker *et al*., 2006). However, the proportions of the contributions from lands and oceans are different among these inversions, with $-0.32 \pm 0.75$ Pg C $yr^{-1}$ attributed to lands in this inversion, $-1.25 \pm$

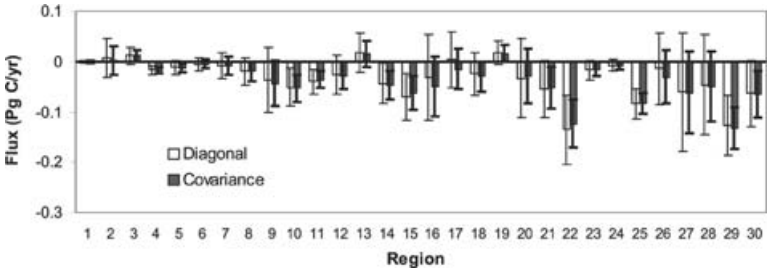


*Fig 6.* Considering the similarity of meteorological conditions among the 30 regions in North America by adding realistic correlations to the a priori flux covariance matrix made a small difference in the carbon source and sink distribution. 'Diagonal': only variance terms in the diagonal of the matrix are considered; 'Covariance': both diagonal and off-diagonal terms are included through considering the meteorological similarity (eq. 6).

0.61 and $-1.75$ Pg C yr$^{-1}$ in the seasonal (1992–1996) and interannual (in 2003) TransCom 3 inversions, respectively. The corresponding ocean surface fluxes are $-2.44 \pm 0.51$ Pg C yr$^{-1}$, $-1.55 \pm 0.61$ Pg C yr$^{-1}$ (1992–1996) and $-0.71$ Pg C yr$^{-1}$.

What are the reasons for the striking differences of land and ocean total fluxes, especially between the result of this inversion and that of TransCom 3 interannual inversion? Sites selection may be one of them. We can see from Fig. 5 that the tropical zone and middle latitude zone in the southern hemisphere contribute the most to the large difference. As we have mentioned, the Easter Island site may cause the flux value to decrease dramatically in the South pacific region (43) and the flux value in the South America region (32) to increase as compensation. The sites we selected in and around the Africa continent are likely to affect the flux over Africa and further contribute to other tropical regions. Patra et al. (2005) used those sites in their inversion and obtained 10-yr (1991–2000) mean fluxes of $-0.31$ and $-2.35$ Pg C yr$^{-1}$ for land and ocean, respectively. Another possible reason is the wind field we used in the forward modelling. As described in Section 2.2, NCEP/NCAR reanalysis dataset for the period of 1999 to 2003 has been used in our modelling. TranCom 3 interannual inversion, however, used the climatological wind field, and 2003 is not a normal year in terms of meteorological conditions (NCDC, 2004). Comparing to TransCom 3 results, the total land carbon uptake decreases considerably, but northern lands are still the largest sinks. North America is a sink of $-0.97 \pm 0.21$ Pg C yr$^{-1}$, while Canada alone is $-0.34 \pm 0.14$ Pg C yr$^{-1}$. The carbon exchange of Canada's forest, grassland and farmland, and Tundra is $-0.33 \pm 0.14$ , $0.02 \pm 0.04$ and $-0.03 \pm 0.02$Pg C yr$^{-1}$, respectively.

In order to use as many sites as possible in North America, we choose to use the GLOBALVIEW-$CO_2$ 2005 dataset in which tower data are now averaged using afternoon hours only. However, monthly mean planetary boundary layer (PBL) heights were used in the NIES model to produce the transport matrices in this study. This incompatibility between model and data may have caused biases towards sink in the inverted fluxes in regions that are tightly constrained by the tower data because the $CO_2$ concentration in the afternoon is much smaller than the daily average. To remove these biases, a transport model capable of using diurnal PBL information is needed in our future study.

## 4. Conclusion

We made an attempt, using a Bayesian synthesis inversion technique, to infer the global seasonal variation of the carbon flux within a nested framework of 50 regions including 30 small regions in North America and 20 large regions of the globe. The main conclusions are as follows.

(1) Based on the uncertainty reduction from the prior to posterior carbon flux, this inversion has made an effective use of atmospheric $CO_2$ observations for improving carbon flux estimation of the various regions. The improvement is uneven across all the 50 regions. Large regions generally have large uncertainty reductions as a whole because of the relatively large numbers of effective constraining observation sites per region. In North America, the uncertainty reductions are larger for regions at middle latitudes where more sites are available for constraining the inversion. Additional three to four observation sites in North America could further improve the nested inversion accuracy.

(2) The annual carbon fluxes from this study are similar to those of TransCom 3 (1992–1996) in the northern hemisphere, although in Europe the carbon exchange was affected by the extreme weather in 2003. Considerable differences exist between TransCom 3 inversions for 1992–1996 and this inversion for 2003 in several other regions. These differences may be partially attributed to the changes in the intensive land use in tropical and southern land regions (FAO, 2005), frequent climate anomalies, and the post-Pinatubo uptake in 1992 (Rödenbeck et al., 2003). The selection of different observation sites in different inversions may account for some of the flux differences in regions where observations are limited.

(3) In North America, the use of 30 small regions based on land cover types could theoretically improve the inversion accuracy through reducing surface heterogeneity within a region. In practice, it is difficult to evaluate this improvement. However, we are quite encouraged by the facts that the inverted flux spatial pattern is mostly consistent with the bottom-up ecosystem modelling results (Chen et al., 2003) and that the use of a prior flux uncertainty covariance matrix with more realistic correlations has made some meaningful modification to the inverted flux distribution. These facts suggest that the nested inversion technique may be a promising way to improve regional carbon cycle estimation.

(4) Large deviations ($>1\sigma$) of inverted fluxes from the prior fluxes show that some prior flux values and uncertainties in the winter and summer in some regions are unreasonable, indicating that further improvements could be made by selecting a realistic a priori flux field and by defining its uncertainties based on physical and biological principles.

## 5. Acknowledgement

This research was supported by a research grant from the Canadian Foundation of Climate and Atmospheric Sciences. The authors thank A. Michalak for her useful discussion and comments and D. Baker and K. Gurney for kindly providing their inversion results for comparison. We thank two anonymous reviewers for their very helpful comments.

## References

Baker, D. F., Law, R. M., Gurney, K. R., Rayner, P., Peylin, and co-author. 2006. TransCom 3 inversion intercomparison: Impact of transport model errors on the interannual variability of regional $CO_2$ fluxes, 1988–2003. *Global Biogeochem. Cycles:* **20**(1), GB1002.

Bousquet, P., Peylin, P., Ciais, P., Le Quéré, C., Friedlingstein, P., and co-authors. 2000. regional changes in carbon dioxide fluxes of land and oceans Since 1980. *Science* **290**, 1342–1346.

Brenkert, A. L. 1998. Carbon dioxide emission estimates from fossil-fuel burning, hydraulic cement production, and gas flaring for 1995 on a one degree grid cell basis, http://cdiac.esd.ornl.gov/ndps/ndp058a.html, Carbon Dioxide Inf. Anal. Cent., Oak Ridge, Natl. Lab., Oak Ridge, Tenn.

Ciais, P., Reichstein, M., Viovy, N., Granier, A., Ogée, and co-authors. 2005. Europe-wide reduction in primary productivity caused by the heat and drought in 2003. *Nature* **437**, 529–533.

Chen, J. M., Chen, W., Liu, J. and Cihlar, J. 2000. Annual carbon balance of Canada's forests during 1985-1996. *Global Biogeochem. Cycles* **14**, 839–850.

Chen, J. M., Ju, W., Cihlar, J., Price, D., Liu, J. W. Chen, and co-authors. 2003. Spatial distribution of carbon sources and sinks in Canada's forests. *Tellus* **55B**, 622–641.

DeFries, R. S. and Townshend, J. R. G. 1994. NDVI-derived land cover classification at a global scale. *Int. J. Remote Sens.* **15**, 3567–3586.

Enting, I. G. 2002. *Inverse Problems in Atmospheric Constituent Transport*. Cambridge Univ. Press, New York.

Enting, I. G., Trudinger, C. M. and Francey, R. J. 1995. A synthesis inversion of the concentration and $^{13}C$ of atmospheric $CO_2$. *Tellus* **47B**, 35–52.

Fan, S., Gloor, M., Mahlman, J., Pacala, S., Sarmiento, J., and co-authors. 1998. A large terrestrial carbon sink in north america implied by atmospheric and oceanic carbon dioxide data and models. *Science* **282**, 442–446.

Food And Agriculture Organization of the United Nations. 2005. Global Forest Resources Assessment 2005, http://www.fao.org/forestry/.

GLOBALVIEW-$CO_2$ 2005. cooperative atmospheric data integration project – carbon dioxide. CD-ROM, NOAA CMDL, Boulder, Colorado [Also available on Internet via anonymous FTP to ftp.cmdl.noaa.gov, Path: ccg/co2/GLOBALVIEW].

Gruber, N., Mikaloff-Fletcher, S. E., Jacobson, A. R., Gloor, M., Sarmiento, J. L., and co-authors. 2005. Oceanic sources and sinks for atmospheric $CO_2$. In: Proceedings of the 7th International Carbon Dioxide Conference, 25–30 September, 2005, Boulder, Colorado, 11–12.

Gurney, K. R., Law, R. M., Denning, A. S., Rayner, P. J., Pak, B. C., and co-authors. 2004. Transcom 3 inversion intercomparison: Model mean results for the estimation of seasonal carbon sources and sinks. *Global Biogeochem. Cycles* **18**(1), GB1010.

Gurney, K. R., Law, R. M., Denning, A. S., Rayner, P. J., Baker, D., and co-authors. 2003. TransCom 3 $CO_2$ inversion intercomparison: 1. Annual mean control results and sensitivity to transport and prior flux information. *Tellus* **55B**, 555–579.

Ju, W. M., Chen, J. M., Black, T. A., Barr, A. G., Mccaughey, H., and co-authors. 2006. Hydrological effects on carbon cycles of Canada's forests and wetlands. *Tellus* **B58**(1), 16–30.

Kalnay, E., Kanamitsu, M., Kistler, R., Collins, W., Deaven, D., and co-authors. 1996. The NCEP/NCAR 40-year reanalysis project. *Bull. Am. Met. Soc.* **77**, 437–471.

Kaminski, T., Heimann, M. and Giering, R.. 1999. A coarse grid three-dimensional global inverse model of the atmospheric transport: 1. Adjoint model and Jacobian matrix. *J. Geophys. Res.* **104** (D15), 18535–18554.

Kaminski, T., Rayner, P. J., Heimann, M. and Enting, I. G.. 2001. On aggregation errors in atmospheric transport inversions. *J. Geophys. Res.* **106**(D5), 4703–4715.

Keeling, C. D., Piper, S. C. and Whorf, T. P.. 2005. A 50 year record of the evolution of the meridional gradient in atmospheric $CO_2$ and its relation to fossil fuel emissions. In: Proceedings of the 7th International Carbon Dioxide Conference, 25–30 September 2005, Boulder, Colorado, 21–22.

Kurz, W. A. and Apps, M. J. 1999. A 70-yr retrospective analysis of carbon fluxes in the Canadian forest sector. *Ecol. Model.* **9**, 526–547.

Law, R. M., Chen, Y.-H., Gurney, K. R. and TransCom 3 modelers. 2003. TransCom 3 $CO_2$ inversion intercomparison: 2. Sensitivity of annual mean results to data choices. *Tellus* **55B**, 580–595.

Liu, J., Chen, J. M., Cihlar, J. and Chen, W. 1999. Net primary productivity distribution in BOREAS region from a process model driven by satellite and surface data. *J. Geophy. Res.* **104**, 27735–27754.

Maksyutov, S. and Inoue, G. 2000. Vertical profiles of radon and $CO_2$ simulated by the global atmospheric transport model, CGER supercomputer activity report,CGER/NIES-I039-2000 **7**, 39–41.

Marland, G., Boden, T. A. and Andres, R. J. 2006. Global, regional, and national $CO_2$ emissions In: Trends: A Compendium of Data on Global Change. Carbon Dioxide Information Analysis Center, Oak Ridge National Laboratory, U.S. Department of Energy, Oak Ridge, Tenn, USA

Masarie, K. A. and Tans, P. P. 1995. Extension and integration of atmospheric carbon dioxide data into a globally consistent measurement record. *J. Geophy. Res.* **100**, D11593–11610.

Michalak, A. M., Bruhwiler, L. and Tans, P. P.. 2004. A geostatistical approach to surface flux estimation of atmospheric trace gases. *J. Geophys. Res.* **109**, D14109.

National Climatic Data Center 2004. Climate of 2003, Annual Review, Significant U.S. and Global Events. http://www.ncdc.noaa.gov/oa/climate/research/2003/ann/events.html

Patra, P. K., Maksyutov, S., Ishizawa, M., Nakazawa, T., Takahashi, T., and co-authors. 2005. Interannual and decadal changes in the sea-air $CO_2$ flux from atmospheric $CO_2$ inverse modelling. *Global Biogeochem. Cycles* **19**, GB4013.

Potter, C., Klooster, S., Myneni, R., Genovese, V., Tan, P.-N., and co-authors. 2003. Continental-scale comparisons of terrestrial carbon sinks estimated from satellite data and ecosystem modeling 1982-1998. *Global Planet. Change* **39**(3–4), 201–213.

Potter, C. S. and Klooster, S. A. 1999. Dynamic global vegetation modeling (DGVM) for prediction of plant functional types and biogenic trace gas fluxes. *Global Ecol. Biogeogr. Lett.* **8**(6), 473–488.

Rödenbeck, C., Houweling, S., Gloor, M. and Heimann, M. 2003. $CO_2$ flux history 1982-2001 inferred from atmospheric data using a global inversion of atmospheric transport. *Atmos. Chem. Phys.* **3**, 1919–1964.

Rayner, P. J., Enting, I. G., Francey, R. J. and Langenfelds, R.. 1999. Reconstructing the recent carbon cycle from atmospheric $CO_2$, $^{13}C$ and $O_2/N_2$ observations. *Tellus* **51B**, 213–232.

Running, S. W. and Coughlan, J. C. 1988. A general model of forest ecosystem processes for regional applications, I. Hydrologic balance, canopy gas exchange and primary production processes. *Ecol. Model.* **42**, 125–154.

Running, S. W. and Gower, S. T.. 1991. FOREST-BGC, a general model of forest ecosystem processes for regional applications, II. Dynamic carbon allocation and nitrogen budgets. *Tree Physiol.* **9**, 147–160.

Sellers, P. J., Mintz, Y., Sud, Y. C., and Dalcher, A.. 1986. A simple biosphere model (SiB) for use within general circulation models. *J. Atmos. Sci.* **43**, 505–531.

Sellers, P. J., Randall, D. A., Collatz, G. J., Berry, J. A., Field, C. B., and co-authors. 1996. A revised land surface parameterization (SiB2) for atmospheric GCMs .1. Model formulation. *J. Climate* **9**, 706–737.

Takahashi, T., Wanninkhof, R., Feely, R. A., Weiss, R. F., Chipman, D. W., and co-authors. 1999. Net sea-air CO2 flux over the global oceans: An improved estimate based on the sea-air pCO2 difference. In Proceedings of the *2nd International Symposium on CO2 in the Oceans*, the 12th global environment Tsukuba, 18-22 January 1999, Tsukuba, Japan, 18-01, 4 pp.

Thornton, P. E., Law, B. E., Gholz, H. L., Clark, K. L., Falge, E., and co-authors. 2002. Modeling and measuring the effects of disturbance history and climate on carbon and water budgets in evergreen needleleaf forests. *Agric. For. Meteorol.* **113**, 185–222.

Wofsy, S. C., Goulden, M. L., Munger, J. W., Fan, S. M., Bakwin, P. S., and co-authors. 1993. Net exchange of $CO_2$ in a midlatitude forest. *Science* **260**, 1314.

Yuen, C. W., Higuchi, K. and TransCom 3 modelers. 2005. Impact of Fraserdale $CO_2$ observation on annual flux inversion of the North America boreal region. *Tellus* **57B**, 203–209.

Zhang, X., Nakazawa, T., Aoki, S., Nakaoka, S., Ishizawa, M., and co-authors. 2005. Temporal variations of the atmospheric $CO_2$ concentration in the southernmost part of Japan. In: Proceedings of the 7th International Carbon Dioxide Conference, 25–30 September 2005, Boulder, Colorado, 425–426.